KINEMATIC AND DYNAMIC ANALYSIS OF A
SPATIAL ONE-DOF FOLDABLE TENSEGRITY MECHANISM

M. A. Swartz[1],   M.J.D. Hayes[2]

[1] *Mechanical and Aerospace Engineering, Carleton University, mark.a.swartz@gmail.com*

[2] *Mechanical and Aerospace Engineering, Carleton University, jhayes@mae.carleton.ca*

Abstract

This paper presents a mechanical analysis of a spatial 1-DOF tensegrity mechanism created by connecting three planar tensegrity mechanisms to form a triangular prism. The subsequent investigation produces kinematic and dynamic models that allow the workspace-boundary singularities and minimum energy configuration to be determined. The singularities are found to occur when the mechanism is folded in the vertical $[X, Y]$ plane or in the horizontal $[X, Z]$ plane. The minimum energy configuration, formed by the angle between the horizontal plane and the actuated strut, is found to be $\theta = \frac{\pi}{4}$. However, when the system is linearized to determine the analytic solution for the dynamics, the minimum energy configuration becomes $\theta = 1$ due to the inherent error produced when the system is linearized. The dynamic response of the mechanism to an initial small displacement is determined for each case of a critically damped, overdamped, and underdamped system.

Keywords: tensegrity; foldable mechanisms; deployable mechanisms; kinematic model; dynamic model.

ANALYSE MÉCANIQUE D'UN MÉCANISME PLIABLE SPATIAL DE 1-DOF
TENSEGRITY

Résumé Cet article présente une analyse mécanique d'un mécanisme spatial du tensegrity 1-DOF créé en reliant trois mécanismes planaires de tensegrity pour former un prisme triangulaire. La recherche suivante produit les modèles cinématiques et dynamiques qui permettent les singularités de zone de travail-frontière et la configuration minimum d'énergie à déterminer. Les singularités s'avèrent pour se produire quand le mécanisme est plié dans [X, Y] l'avion vertical ou dans le plan [X,Z] horizontal. La configuration minimum d'énergie s'avère $\theta = \frac{\pi}{4}$, qui est l'angle entre le plan horizontal et la contrefiche actionnée. Cependant, quand le système est linéarisé pour déterminer une solution analytique pour la dynamique, la configuration minimum d'énergie devient $\theta = 1$ dû à l'erreur inhérente dans la linéarisation du système. La réponse dynamique du système à un premier déplacement est déterminée pour chaque cas en critique d'atténué, overdamped, ou underdamped des systèmes.

Mots clés: tensegrity; mécanismes pliables; mécanismes déployables; modèle cinématique; modèle dynamique.

1 INTRODUCTION

The application of tensegrity structures to foldable, lightweight, and highly accurate controllable mechanisms is a natural evolution of the almost fifty year old concept, evidenced by active research projects worldwide [1],[2],[3],[4]. Tensegrity structures can be defined as self-equilibrating structures based on a network of compressed struts and tensioned cables.

A foldable tensegrity mechanism can be designed by mechanically actuating one or more elements of the tensegrity network of cables and struts [5]. Deployable tensegrity mechanisms have been applied to foldable arrays, antennas, booms [6], space structures [2], truss systems, and tendon-driven robots arms [7],[8]. Future applications may even include aeronautical and medical devices.

This paper presents a mechanical analysis of a spatial 1-DOF tensegrity mechanism created by connecting three planar tensegrity mechanisms to form a triangular prism. The subsequent investigation generates a simple kinematic and dynamic model which are used to determine the workspace singularities of the system and the minimum energy configuration. The system response to initial displacements is also investigated to verify the dynamic model.
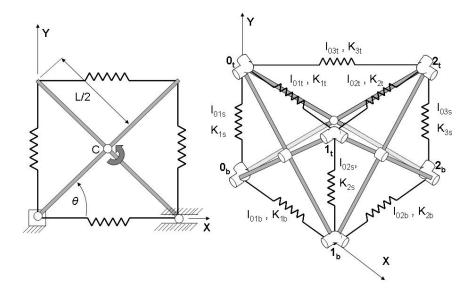
2 TENSEGRITY MECHANISM KINEMATIC ARCHITECTURE

Figure 1: Planar (left) and spatial (right) tensegrity mechanisms.

The spatial 1-DOF tensegrity mechanism shown in Figure 1 is composed of three planar tensegrity mechanisms (left) connected together to form a prism (right). The top and bottom face of the prism form an equilateral triangle and therefore each of the side faces are separated by $60°$. At each of the prism corners two struts join together forming a node. Thus, there are six nodes altogether. Using the Chebyshev-Grübler-Kutzback (CGK) formula, the joint configuration at each node is selected to ensure that the total number of degrees of freedom (DOF) for the mechanism is one.

2.1 Mechanism Design Parameters

The 1-DOF spatial tensegrity mechanism is shown in Figure 1 and consists of six struts of length L assembled into three planar mechanisms. Each planar mechanism consists of two struts connected by a revolute joint at length $L/2$. The three planar mechanisms are joined at six nodes labeled $[0_b, 1_b, 2_b]$ for the bottom face of the prism and $[0_t, 1_t, 2_t]$ for the top face. Between each node along the base (b), side (s), and top (t) an elastic element is placed of length l_{0kp} and linear stiffness K_{kp} where $k \in \{1, 2, 3\}$ and $p \in \{b, s, t\}$. For the following analysis, it will be assumed that $l_0 = l_{0kp}$ $\forall\, [k, p]$, $K = K_{kp}$ $\forall\, [k]$, where $p \in \{b, t\}$. For the elastic elements on the sides, $2K = K_{ks}$ $\forall\, [k]$. Mechanism damping will be modeled for each of the three revolute joints with linear damping coefficient C. All other joints are assumed frictionless.

Since the system possesses 1-DOF, actuating the mechanism could be accomplished by replacing any of the elastic elements with an inextensible cord that could be coiled and uncoiled. The resulting contraction between any two nodes would be mimicked throughout the mechanism causing it to expand or contract. Alternatively, an actuator could vary the angle θ as measured from the horizontal plane at the base to one of the struts, resulting in the same mechanism expansion-contraction response. The following analysis will be performed on the unactuated mechanism. It will focus on the $[X, Y]$ plane by placing an inertial coordinate system at the fixed base joint labeled node 0_b, with the Y-axis extending from node 0_b to 0_t and the x-axis from 0_b to 1_b.

2.2 Mobility Analysis

The planar tensegrity mechanism shown in Figure 1 is constrained to move in the $[X, Y]$ plane and thus the axis of rotation for each joint must be normal to that plane. When three planar mechanisms are connected together to create the spatial system, the normal revolute axis for each neighbouring strut is separated by an angle of $60°$ and thus the joints at each of the six nodes must allow rotation about these two axes so that the planar faces remain planar. Therefore, the joint at each node is a universal joint, J_2, since four constraints are imposed.

It was demonstrated by Arsenault and Gosselin that a similar planar mechanism could have up to 2-DOF provided that the struts were permitted to slide relative to one another [3], [9]. Therefore, to remove this DOF, a J_1 revolute joint was placed at the centre of each strut.

Using the CGK formula, the DOF of the tensegrity mechanism can be verified:

$$DOF = d(n-1) - \sum_{i=1}^{j} U_i - m \tag{1}$$

where d is the dimension of the motion space for each unconstrained link, j is the total number of joints, m is the number of idle DOF, n is the number of links (struts), and U_i is the number of constraints for the ith joint.

Setting the following values in the CGK formula yields the mechanisms mobility: $d = 6$, $J_1 = 3$, $J_2 = 6$, $m = 0$, and $n = 7$ (6 struts and the ground). The CGK formula yields -3 which signifies an indeterminant structure. To achieve the 1-DOF required, four of the universal joints will be replaced by spherical J_3 joints. The final joint configuration is shown in Figure 2.

For the tensegrity mechanism shown in Figure 2, $d = 6$, $J_1 = 3$, $J_2 = 2$, $J_3 = 4$, thus $j = 9$.
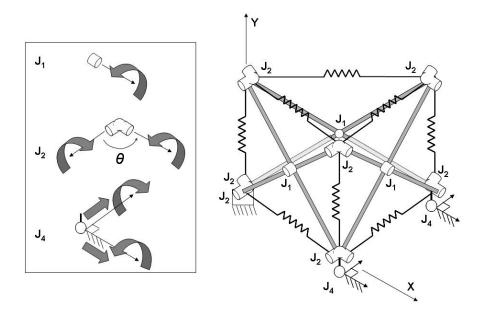
Figure 2: Spatial 1-DOF tensegrity mechanism and associated joints.

There are no idle DOF so $m = 0$. The links include six struts and the ground, therefore $n = 7$ (since there is no interaction between the springs at the joints they can be neglected). Finally, the revolute joints impose five constraints, the universal joints impose four constraints, and the spherical joints impose three constraints. Thus U_i is five, four, and three for each of the corresponding i^{th} links. The CGK formula yields

$$DOF = 6(7 - 1) - 5J_1 - 4J_2 - 3J_3 = 1. \tag{2}$$

3 KINEMATIC MODEL

The kinematic model can be easily determined from the geometry of the mechanism. As the mechanism is 1-DOF, only one of the three identical planar faces need be considered. Using the $[X, Y]$ plane previously described, the analysis of the kinematics will provide the Jacobian which will be used to determine the singular configurations of the mechanism.

3.1 Geometric Analysis

From Figure 1 it is clear that the total displacements along the X and Y axes are related to the angular displacement, θ, by

$$x = Lcos\theta, \;\; y = Lsin\theta. \tag{3}$$

Combining the above expressions yields the output displacement, y, in terms of the input displacement, x:

$$y = \sqrt{L^2 - x^2}. \tag{4}$$

The plot of Equation (4) shown in Figure 3 (left) produces the mechanism workspace. Differentiating Equation(4) twice more yields the velocity and acceleration equations

$$\dot{y} = \frac{-x}{\sqrt{L^2 - x^2}}\dot{x} = \mathbf{J}\dot{x}, \tag{5}$$

$$\ddot{y} = \frac{-1}{\sqrt{L^2 - x^2}}\left(\ddot{x} + \left(1 + \frac{x^2}{L^2 - x}\right)\frac{\dot{x}^2}{x}\right). \tag{6}$$

Equation (5) is a function of the mechanisms 1×1 Jacobian, $\mathbf{J}$, which transforms the input velocity along the X-axis, $\dot{x}$, to the output velocity along the Y-axis, $\dot{y}$.

3.2 Singularity Analysis

In general, the Jacobian is a multidimensional form of the derivative for which singularities occur when it is no longer invertible [10]. This condition occurs when the determinant $det(\mathbf{J}) = 0$ or $det(\mathbf{J}) \to \infty$. Since the Jacobian of the tensegrity mechanism is a 1×1 matrix, its determinant is itself and the singular configurations are easily determined from Equation (5) as $x = 0$ and $x = L$. These values for x correspond to $\theta = 0$ and $\theta = \frac{\pi}{2}$ via Equation (3). Using these results in Equation(4) yields the resulting value for y. For $x = 0$ and $x = L$ these are, respectively

$$\begin{aligned} Case\ 1 &: x = 0\ \ or\ \ \theta = 0; \quad y = L, \\ Case\ 2 &: x = L\ \ or\ \ \theta = \tfrac{\pi}{2}; \quad y = 0. \end{aligned} \tag{7}$$

These singularities are workspace-boundary singularities since they occur when the tensegrity is fully extended in the X and Y directions as shown in Figure 3. In these configurations the struts overlap. In Case 1, the struts are folded vertically resulting in the gain of an instantaneous DOF causing the mechanism to tip over at the fixed base joint. Momentarily considering an actuator
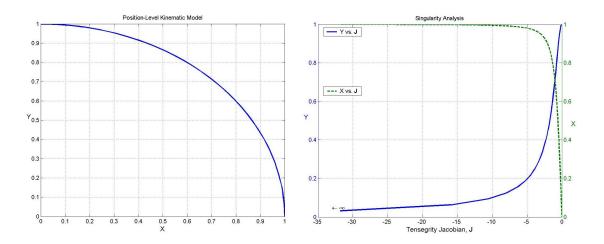

Figure 3: Tensegrity mechanism workspace (left) and singular configurations (right) with L = 1.

placed along the X-axis, it would only have to provide an infinitesimal amount work to expand the mechanism, and as well, it could not resist any perturbation causing the mechanism to expand along the X-axis. For Case 2, the mechanism is folded horizontally resulting in the instantaneous loss of a DOF and transforming the mechanism into a structure. The actuator would have to provide an infinite amount of work along the X-axis in order to expand the tensegrity vertically.

From Figure 3, the equilibrium position can be determined from the intersection of the curves. This point is the configuration where the input and output displacements are equal,

$$y = x = \frac{\sqrt{2}}{2}, \tag{8}$$

which requires that $\mathbf{J} = 1$ in Equation (5). This corresponds to a strut angle of $\theta = \frac{\pi}{4}$.

4 DYNAMIC MODEL

In the following section, the dynamic model of the tensegrity mechanism will be developed using the Lagrange formulation. It has been shown that this system has 1-DOF and therefore has a single generalized coordinate, θ, that defines the motion. The generalized coordinate also defines the three spatial coordinates as follows:

$$x = Lcos\theta, \;\; y = Lsin\theta, \;\; z = -Lcos\theta cos30°. \tag{9}$$

4.1 The Equation of Motion

The well known Lagrange equation of motion is formulated in terms of the derivatives of the kinetic and potential energy of the system with respect to the generalized coordinates, q_i.

$$\frac{d}{dt}\left(\frac{\delta}{\delta \dot{q}_i}T\right) - \frac{\delta}{\delta q_i}T + \frac{\delta}{\delta q_i}V = Q_i. \tag{10}$$

where T, V, and , Q_i are the kinetic, potential, and generalized forces of the system and i is the number of generalized coordinates. For the 1-DOF tensegrity mechanism, $i = 1$, and thus only one generalized coordinate is required: $q_1 = \theta$.

The total kinetic energy, T, for all $n = 6$ translating and rotating struts of mass m_j and moment of inertia Io_j, where $m = m_j$ and $Io = Io_j \; \forall \; j$, is the sum of kinetic energy for each strut, j;

$$T = \frac{1}{2}\sum_{j=1}^{n} Io_j \dot{\theta}_j^{\,2} + m_j v_j^2. \tag{11}$$

The total potential energy, V, and its gravitational and elastic components, Ω and U, are given respectively by

$$V = \Omega + U, \;\; \Omega = \sum_{j=1}^{n} m_j g\rho, \;\; U = \tfrac{1}{2}\sum_{p}\sum_{k=1}^{3} K_{kp}(\rho - l_{0kp})^2. \tag{12}$$

For the above equations recall the index for the base (b), side (s), and top (t) elastic elements, where $p \in \{b, s, t\}$. For the top and bottom elastic elements $K = K_{kp}$ and for the sides, $2K = K_{kp}$. The parameter $\rho = x$ or $\rho = y$ depending upon whether the X- or Y-direction is being analyzed.

Neglecting non-linear terms, the kinetic energy of the struts is determined to be

$$T = mL^2\dot{\theta}^2. \tag{13}$$

The total potential energy is

$$V = 3mgL\sin\theta + 3K(L\cos\theta - l_0)^2 + 3K(L\sin\theta - l_0)^2. \tag{14}$$

The generalized force, Q_1, associated with the virtual work arises from the damping modeled at the revolute joint of each strut intersection and is defined as

$$Q_1 = -3C\dot{\theta}. \tag{15}$$

Using Lagrange, Equation (10), the non-linear second-order differential equation of motion for the 1-DOF tensegrity mechanism is generated.

$$\ddot{\theta} + \frac{3}{2}\frac{C}{mL^2}\dot{\theta} + \frac{3}{2}\frac{g}{L}\cos\theta + \frac{3Kl_0}{mL}(\sin\theta - \cos\theta) = 0. \tag{16}$$

Using Equation (9) the following relationships can be derived to rewrite the equation of motion in terms of the spatial coordinates x and y.

$$\begin{aligned}
\dot{\theta} &= -\frac{1}{y}\dot{x}, \\
\ddot{\theta} &= -\frac{1}{y}\ddot{x} + \frac{x}{y^2}\dot{x}.
\end{aligned} \tag{17}$$

Thus the equation of motion becomes

$$\ddot{x} + \left(\frac{3}{2}\frac{C}{mL^2} - \frac{x}{y}\right)\dot{x} - \frac{3}{2}\frac{g}{L^2}xy - \frac{3Kl_0}{mL^2}(y - x)y = 0. \tag{18}$$

4.2 Equilibrium Position

The equation of motion can be used to determine the minimum energy configuration of the tensegrity mechanism. This configuration is the equilibrium position which arises when $\ddot{\theta} = \dot{\theta} = 0$ in Equation (16) and all external forces are set to zero. Given these assumptions, only the potential energy of the system contributes to the equilibrium position. Equation (16) reduces to

$$\left(\frac{2Kl_0}{mL}\right)\sin\theta - \left(\frac{2Kl_0}{mL} - \frac{g}{L}\right)\cos\theta = 0. \tag{19}$$

In a system where the stiffness dominates, that is, where K is large, the gravitational component of the potential energy can be neglected, and Equation (19) reduces to

$$\sin\theta - \cos\theta = 0, \tag{20}$$

which is satisfied when $\theta = \frac{\pi}{4}$. Similarly, by setting $\ddot{x} = \dot{x} = 0$ in Equation (18), the equilibrium in terms of the spatial coordinates can be found;

$$y = \left(1 - \frac{gm}{2Kl_0}\right)x. \tag{21}$$

As before, if the stiffness dominates, the gravitational term can be neglected which reduces the above to $y = x$. This corresponds to the previous result obtained in Equation (20). A more rigorous exploration of the equilibrium condition of tensegrity structures is provided by Williamson *et al.* [11].

4.3 Linearization of the Equation of Motion

In order to find an analytic solution for Equation (16) it must first be linearized by assuming small mechanism deflections and approximating the non-linear terms. This is accomplished by setting $cos\theta = 1$ and $sin\theta = \theta$. The linear second-order differential equation is then

$$\ddot{\theta} + \frac{3}{2}\frac{C}{mL^2}\dot{\theta} + \frac{3Kl_0}{mL}\theta = \frac{3}{2L}\left(\frac{2Kl_0}{m} - g\right). \tag{22}$$

4.4 The Steady-State Solution

Using the linear differential equation of motion, the steady-state, or particular solution, can be derived. The time-invariance of the right-hand side term of Equation (22) indicates that the steady-state solution is a constant value to which the transient solution will converge. Taking this steady-state value to be θ_s,

$$\dot{\theta}_s = \ddot{\theta}_s = 0. \tag{23}$$

Substituting this result back into the linear differential equation produces the steady-state solution.

$$\theta_s = 1 - \frac{mg}{2Kl_0}. \tag{24}$$

This result represents the equilibrium condition to which the system would converge when $\ddot{\theta} = \dot{\theta} = 0$. The expression is similar to the result obtained in Equation (21) where the system was shown to have an equilibrium at $\frac{\pi}{4}$ rads. However, because the differential equation was linearized, the system will converge instead to $\theta_s = 1$ rad, or $57.3°$, assuming that the stiffness is large.

4.5 The Transient Solution

The solution to the homogeneous equation represents the transient response of the system to an initial displacement. The homogeneous equation is

$$\ddot{\theta} + \frac{3}{2}\frac{C}{mL^2}\dot{\theta} + \frac{3Kl_0}{mL}\theta = 0. \tag{25}$$

Using the following standard substitution, $\theta = Ae^{pt}$, in terms of some constant, A, determined from initial conditions, and p determined from the systems physical parameters, Equation (25) can be expressed in terms of the systems natural frequency, ω_n, and damping coefficient, ζ:

$$p^2 + 2\zeta\omega_n p + \omega_n^2 = 0, \tag{26}$$

where

$$\omega_n^2 = \frac{3Kl_0}{mL}, \quad \zeta = \frac{C}{C_{cr}} = \frac{C}{\sqrt{\frac{16}{3}KmL^3 l_0}}. \tag{27}$$

The solution to Equation (26) is obtained using the quadratic formula,

$$p_1 = -\zeta\omega_n + \omega_n\sqrt{\zeta^2 - 1}, \quad p_2 = -\zeta\omega_n - \omega_n\sqrt{\zeta^2 - 1}. \tag{28}$$

Three classes of solution of Equation (26) exist depending on the value of ζ. These are the critically damped, overdamped, and underdamped cases corresponding to $\zeta = 1$, $\zeta > 1$, and $\zeta < 1$ respectively. The homogenous solution for each case is as follows:

$$\begin{aligned}
\theta_{CD_h} &= A_1 e^{-\omega_n t} + A_2 t e^{-\omega_n t}, \\
\theta_{OD_h} &= B_1 e^{-\omega_n t} + B_2 e^{-\omega_n t}, \\
\theta_{UD_h} &= e^{-\zeta\omega_n t}\left(C_1 cos\omega_n\sqrt{1-\zeta^2}t + C_2 sin\omega_n\sqrt{1-\zeta^2}t\right).
\end{aligned} \tag{29}$$

The complete solution is obtained from the sum of the homogeneous and steady-state solutions. Defining the initial conditions to be $\theta(0) = \theta_0$ and $\dot{\theta}(0) = 0$, the complete solution for the critically damped, $\theta_{CD}(t)$, overdamped, $\theta_{OD}(t)$, and underdamped, $\theta_{UD}(t)$, cases are, respectively

$$\theta_{CD}(t) = (\theta_0 - \theta_s)e^{-\omega_n t} + \omega_n(\theta_0 - \theta_s)t e^{-\omega_n t} + \theta_s, \tag{30}$$

$$\theta_{OD}(t) = \left(\frac{\theta_s - \theta_0}{2\omega_n\sqrt{\zeta^2 - 1}}\right)p_2 e^{-\omega_n t} + (\theta_0 - \theta_s)\left(1 + \frac{p_2}{2\omega_n\sqrt{\zeta^2 - 1}}\right)e^{-\omega_n t} + \theta_s, \tag{31}$$

$$\theta_{UD}(t) = e^{-\zeta\omega_n t}\left((\theta_0 - \theta_s)cos\omega_n\sqrt{1-\zeta^2}t + (\theta_0 - \theta_s)\left(\frac{\zeta}{\sqrt{1-\zeta^2}}\right)sin\omega_n\sqrt{1-\zeta^2}t\right) + \theta_s. \tag{32}$$

4.6 Model Verification

The dynamic model for the critically damped, overdamped, and underdamped cases are illustrated in Figures 4, 5, and 6. The system values were set to $L = 1$, $l_0 = 0.5$, and $m = 0.05$, with an initial angular displacement of $\theta_0 = \frac{\pi}{6}$. For each case the stiffness of the system was varied through $K = [1 \ 10 \ 100 \ 1000]$.

At each value of K the natural frequency, ω_n, and critical damping coefficient, C_{cr}, were determined using Equation (27). The damping ratio was selected to satisfy the critical-, over-, and underdamped cases, $\zeta = [1 \ 1.6 \ 0.4]$. From these values the mechanism damping, C, could be determined. The calculated model parameters are presented in Tables 1, 2, and 3.

The dynamic model clearly demonstrates that at low stiffness, i.e. $K = 1$, the tensegrity mechanism tends to sag under its own weight. After release, it returns to an equilibrium position just below the initial displacement value. This arises in the steady-state solution where a low stiffness will cause the gravity term to dominate. Conversely, at higher stiffness values, the equilibrium position shifts closer to 1 or $57.3°$, which was determined for the infinitely stiff linearized system.
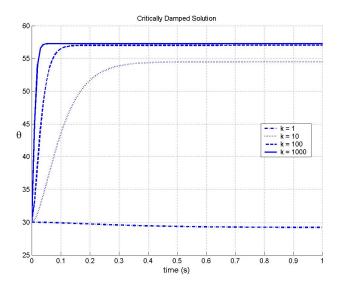
Figure 4: Critically damped: $L = 1, l_0 = 0.5, m = 0.05, \theta_0 = \frac{\pi}{6}$.

Table 1: Calculated Parameters for Critically Damped Case.

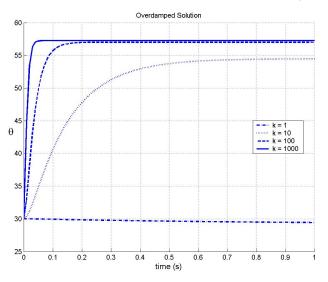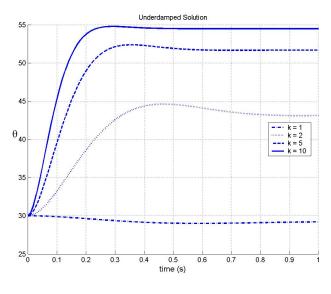| Parameter	Model 1	Model 2	Model 3	Model 4
K	1	10	100	1000
C_{cr}	0.365	1.155	3.652	11.547
C	0.365	1.155	3.652	11.547
ζ	1	1	1	1
ω_n	5.477	17.321	54.772	173.205

Figure 5: Overdamped: $L = 1, l_0 = 0.5, m = 0.05, \theta_0 = \frac{\pi}{6}$.

Table 2: Calculated Parameters for Overdamped Case.

Parameter	Model 1	Model 2	Model 3	Model 4
K	1	10	100	1000
C_{cr}	0.365	1.155	3.652	11.547
C	0.584	1.848	5.842	18.475
ζ	1.6	1.6	1.6	1.6
ω_n	5.477	17.321	54.772	173.205

Figure 6: Underdamped: $L = 1, l_0 = 0.5, m = 0.05, \theta_0 = \frac{\pi}{6}$.

Table 3: Calculated Parameters for Underdamped Case.

Parameter	Model 1	Model 2	Model 3	Model 4
K	1	10	100	1000
C_{cr}	0.365	1.155	3.652	11.547
C	0.146	0.462	1.461	4.619
ζ	0.4	0.4	0.4	0.4
ω_n	5.477	17.321	54.772	173.205

5   CONCLUSIONS

The concept for a 1-DOF spatial tensegrity mechanism was introduced in this paper and the kinematic and dynamic models for small displacements were developed. The first part of the analysis showed that the mechanism possessed a single DOF using the CGK formula. Then the kinematic model was developed which provided insight into the workspace-boundary singularities. These occurred in the $[X, Z]$ plane when $x = L$ and $y = 0$, and in the $[X, Y]$ plane when $x = 0$ and $y = L$. The kinematic model also provided insight as to the location of the equilibrium position. At the condition of $\mathbf{J} = 1$, the input was related to the output via $y = x$, which consequently resulted in $\theta = \frac{\pi}{4}$.

The systems dynamic model was developed using Lagrange's formulation resulting in a non-linear second-order differential equation. For the non-linear system the equilibrium position was determined to be $\theta = \frac{\pi}{4}$. After linearizing the differential equation, a critically damped, over-damped, and underdamped dynamic model was analyzed. All models converged to the mechanism equilibrium or steady-state solution, $\theta_s = 1$, as predicted for a stiff mechanism. This amounts to a $12.3°$ discrepancy between the linear and non-linear models. Thus, since the model was linearized in order to solve the differential equation, it could not be used to provide accurate control over an actuated tensegrity mechanism.

REFERENCES

[1] R. Motro. *Tensegrity: Structural Systems for the Future*. Kogan Page, 2003.

[2] G. Tibert. "Deployable Tensegrity Structures for Space Applications". *Doctoral Thesis, Stockholm*, 2002.

[3] M. Arsenault and C.M. Gosselin. "Development and analysis of a planar 1-DOF tensegrity mechanism". *CSME Forum*, 2004.

[4] R. Skelton, J. Helton, R. Adhikari, J. Pinaud, and W. Chan. "An Introduction to the Mechanics of Tensegrity Strutures". *University of California, San Diego*, 2006.

[5] C. Sultan and R. Skelton. "Deployment of tensegrity structures". *International Journal of Solids and Structures 40 (2003) 4637-4657*, 2003.

[6] J. Pinaud, S. Solari, and R. Skelton. "Deployment of a class 2 tensegrity boom". *University of California, San Diego*, 2002.

[7] J. Aldrich, R. Skelton, and K. Kreutz-Delgado. "Control Synthesis for a Class of Light and Agile Robotic Tensegrity Strutures". *Proceedings of American Control Conference, Colerado*, 2003.

[8] J. Aldrich and R. Skelton. "Control/structure optimization approach for minimum-time reconfiguration of tensegrity systems". *Smart Structures and Materials 2003: Modeling, Signal Processing, and Control*, 2003.

[9] M. Arsenault and C.M. Gosselin. "Kinematic, static, and dynamic analysis of a planar 2-DOF tensegrity mechanism". *Mechanism and Machine Theory 41 (2006) 1072-1089*, 2006.

[10] J. Craig. *Introduction to Robotics: Mechanics and Control*. Pearson - Prentice Hall, third edition, 2005.

[11] D. Williamson, R. Skelton, and J. Han. "Equilibrium Conditions of a Tensegrity Struture". *Proceedings of the 3rd World Conference on Structural Control, Italy*, 2002.